

Wire Extensometer Based on Optical Encoder for Translational Landslide Measurement

Andi Setiono^{a,*}, Qomaruddin^a, M. Imam Afandi^b, Hendra Adinanta^b, Mefina Y. Rofianingrum^a, Suryadi^a, Imam Mulyanto^a, Dwi Bayuwati^a, Arif Anwar^c and Bambang Widiatmoko^a

^a Research Center for Photonics, National Research and Innovation Agency (BRIN), Tangerang Selatan, Indonesia

^b Research Center for Hydrodynamics Technology, National Research and Innovation Agency (BRIN), Surabaya, Indonesia

^c Research and Development Agency of Transportation of the Ministry of Transportation, Jakarta 10110, Indonesia

Corresponding author: *andi.setiono@lipi.go.id

Abstract—A landslide is a natural disaster mostly accompanied by heavy rains, earthquakes, or volcanic eruptions. Due to its significant incurred losses, several studies have been conducted to develop a landslide monitoring system. In this report, we built and implemented optical-based wire-extensometers to measure and monitor a translational landslide in a prone area. This extensometer was built of an optical rotary encoder (whose shaft bonded to a spiral spring and sling rope) interfaced to a low-cost microcontroller as a principal component and subsequently linked to a GSM-based wireless network. The working principle of the employed sensor described in this paperwork is to count optical pulse signal and convert it into a length unit. This sensor can provide much better signal stability and show high resolution for a wide-range measurement than voltage- or current-based sensors. The specification of the engaged optical encoder provides 2000 pulses per rotation, leading to a length resolution of 0.011 ± 0.0083 mm with a speed limit of about 36 mm/s. Furthermore, the wire extensometer was examined in a remote place near a double-track train road to assess its performance in an actual field. A solar cell system was applied as its main power supply. An example of transmitted data shows a land shift from 12 mm to 150 mm, which is mainly triggered by high rainwater infiltration. This result demonstrates that the developed extensometer is deserved to be promoted for landslide monitoring in the geological research-work area.

Keywords— Gateway; landslide; land displacement; remote sensing; wireless sensor network.

Manuscript received 30 Jun. 2021; revised 16 Apr. 2022; accepted 6 Jun. 2022. Date of publication 28 Feb. 2023.
IJASEIT is licensed under a Creative Commons Attribution-Share Alike 4.0 International License.



I. INTRODUCTION

A landslide is a natural disaster defined as a downslope movement of soil, debris, rock, and organic materials under the effects of gravity [1] [2], which acts as a driving force. The landslide also denotes a slope failure that may contribute to soil instability [3]. The incident of landslide, in principle, is triggered by a loss of the adhesive force (i.e., resisting force inside the soil structure), which prevents a movement/sliding of an enormous soil mass. Here, the driving force tends to pull the soil mass downward and equal or exceed the resisting forces that hold the soil mass in place [4]. Landslides are generally classified by type of movement, i.e., slides, flows, spreads, topples, or falls [5–7]. For slides, type is further divided into rotational landslide and translational landslide.

Regarding the type of translational slide, we built an encoder-based wire extensometer to observe a surface-soil displacement by measuring its translational shift. A

translational slide is a type of landslide regolith [8] that occurs mainly in the wet/rainy season. In this slide type, the near-surface soil and rock debris get saturated with water, and subsequent slides, flow downslope and outward along a relatively planar surface. A type of landslide often stimulates a disastrous consequence during concealment [9]. This work was intended to assess the developed landslide sensor and support a landslide monitoring system. There are some considered parameters for landslide analysis and prediction, such as a land tilt [10], water soil [11–13], and mathematical algorithm [14–18], historical slope failure database [19, 20], including surface-soil slide detected using extensometer [21]. A landslide analysis and prediction are necessary for mining vital and densely populated areas. Therefore, this sensor application becomes an essential issue to avoid fatalities and minimize any material losses. Regarding a remote place near a double-track train, a reason for the fast soil movement was investigated using a wire extensometer sensor system. This

measurement involves a rainfall measurement to support the data analysis.

II. MATERIALS AND METHOD

A. Extensometer

We designed a wire extensometer to detect a translational landslide by converting its translational motion to rotational motion. This device was constructed using an optical rotary encoder (Autonics, type of E40S6-2000-3-T-5) as the main component, which inside employs LEDs (light-emitting diodes) light source and photodetectors (Fig. 1 (a)). Both components play a role in converting the angular motion to digital output signals in the form of pulse numbers. The incremental optical encoder is the most widely used of typical rotary encoders due to its low cost and ability to provide signals. Subsequently, the generated signals can be easily interpreted into some parameters such as velocity or change in position. Figure 1 (b) illustrates how the incremental optical encoder provides information on the instantaneous position of a rotating shaft by producing two output square wave cycles per increment of shaft rotation.

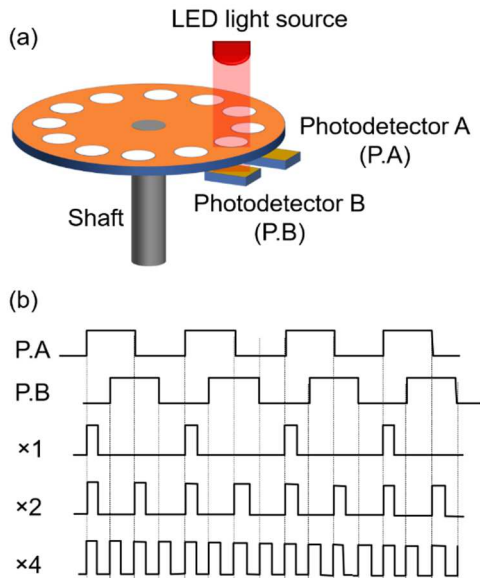


Fig. 1 (a) Schematic of the incremental optical encoder. (b) Quadrature signals with 90 degrees phase differences can lead to quadruple ($\times 4$) the number of pulses per rotation.

These two output wave signals are 90 degrees phase differences, leading to quadrature signals. It is possible to increase the resolution by counting the leading and trailing edges of the quadrature pulses through each photodetector channel, which can further double ($\times 2$) the number of pulses per revolution (ppr). Hence, counting both leading and trailing edges of both channels (i.e., P.A and P.B), a quadrature encoder will quadruple ($\times 4$) the number of pulses per rotation. As a result, if we have 2,000 pulses per rotation (ppr) quadrature encoder, it can be increased to a maximum of 8,000 ppr counter data. It works on voltage-based interpretation compared to multi-turn potentiometer-based extensometers [21] or bending-based fiber optic extensometers. This developed extensometer provides much

better stability and high resolution for wide-range measurement.

As illustrated in Fig. 2, the encoder is harmonized with a metal spring (stainless-steel, $500 \times 5 \times 0.7$ mm) coiled in a spring case and interfaced to wire-roll via a shaft. This mechanical system allows the translational soil motion connected to the wire to be converted to the rotational motion of the rotary encoder. Furthermore, as depicted in Fig. 3, the encoder system is linked to a microcontroller-based system to count the occurred pulse per rotation and interpret it to a sliding parameter in a unit of mm (millimeters). The measured slide was subsequently transmitted through an RF (radio frequency)-based transmitter system to a gateway system which distanced around ~ 500 m from the extensometer's location.

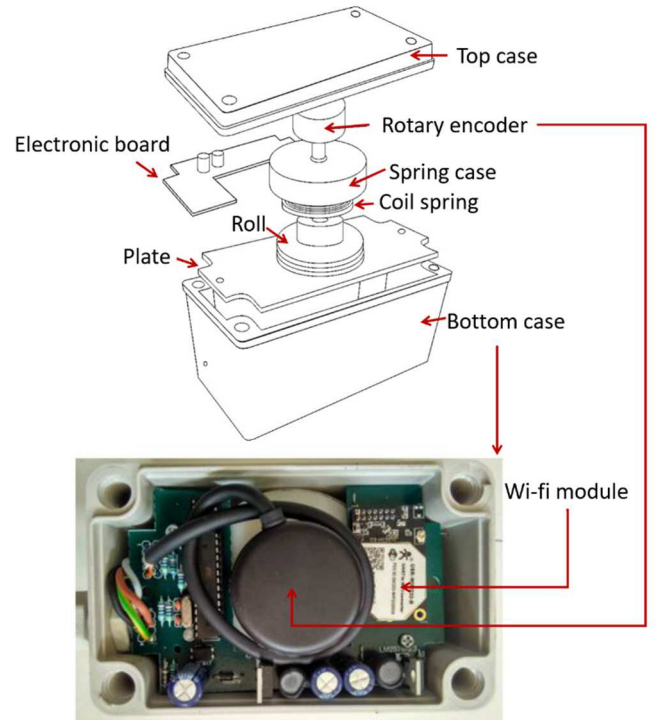


Fig. 2 Schematic design of the extensometer comprised of a rotary encoder, coil spring, and other supporting components.

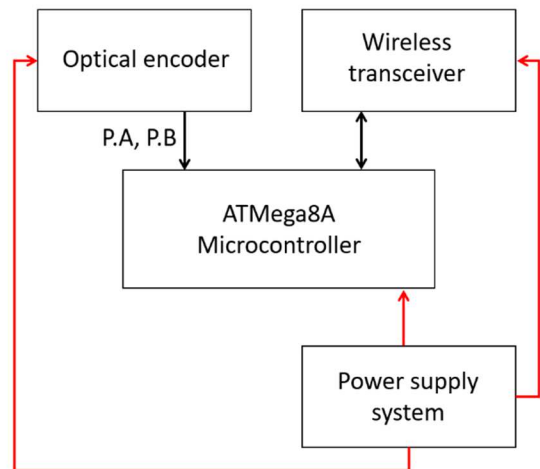


Fig. 3 Schematic of encoder-based extensometer constructed using microcontroller-based signal processing and transmission.

Furthermore, the flowchart path run on the extensometer system is illustrated in Fig. 4. The program written in embedded C language is started by initializing the operated module inside the microcontroller, such as serial, analog to digital converter (ADC), and an inter-integrated circuit (I2C) modules. Afterward, the microcontroller will check up on a coming command and identify the ID number delivered by the gateway system through a radio transceiver connected to the serial module. The measured data will be transmitted to the gateway system if all command parameters are correct. On the contrary, the program will be iterated to the serial port checking if the received ID is incorrect.

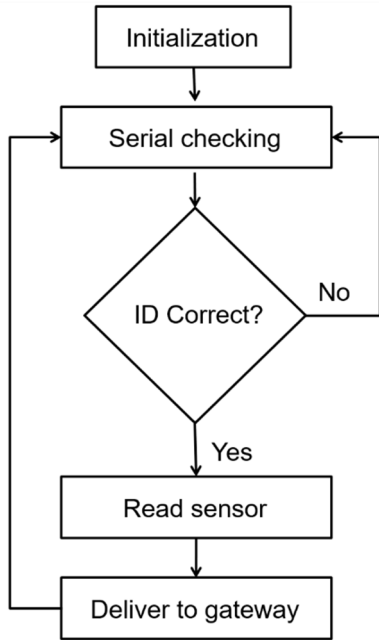


Fig. 4 Programming procedure deployed in extensometer system.

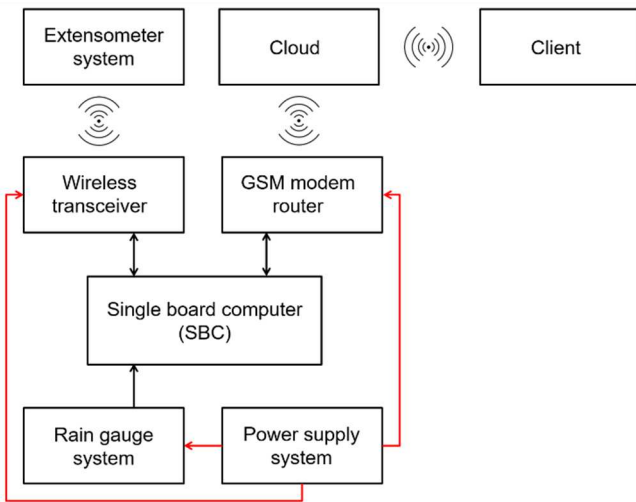


Fig. 5 Schematic of gateway system for transmitting command and requested data to and from extensometer system and delivering the collected data to the data center via GSM network. Besides, the gateway system is featured a rain gauge to measure rainfall levels.

B. Wireless Gateway System

To acquire the measured data from the extensometer, we built a wireless gateway system to collect the measured data and wirelessly transmit them to the data center via a GSM

(Global System for Mobile Communications) network. As delineated in Fig. 5, the gateway system comprises a single-board computer (SBC, NanoPi NEO Plus2) completed with a sub-GHz radio transceiver (XBee-Pro S2C) and an industrial GSM modem router (USR-G781). Moreover, the gateway system is featured a tipping-bucket-based rain gauge system for providing rainfall information. The SBC system's employment is responsible for delivering a command containing data-request and receiving the measured data from the extensometer via the XBee-based system, which is simultaneously packaged with rainfall information. In a certain period of 5 min, the SCB transmits the collected packaged data to the clouds system (data center) through a router system. Furthermore, a web-based user interface is employed in the "final destination"; subsequently, the client can render the graph based on the collected data.

A python-based programming language was configured in the SBC system under a Linux-based operating system and ran continuously in the background. The program was constructed to deliver a request command to the sensor system (extensometer and rainfall counter) and transmit the measured data to the cloud system through TCP-IP communication protocol. Afterward, the measured data can eventually reach the server/client for analysis and evaluation. If the server/client evaluates a danger indication, a response signal will be transmitted to the gateway to enable a danger alarm.

C. Power System

Utilizing a ray of rich sunshine in the observation location, a solar cell-based energy source was employed to provide the electric power. Indonesia as a country located on the equator is known for its abundance of sunny days, with average radiation intensity of about 4.8 kWh/m² a day and an average of ~12 hours per day of radiation length [22]. The case observation area of this work in Purwakarta Regency has direct normal irradiation (DNI) of 3.047 kWh/m² per day. Moreover, an amount of power of 3.902 kWh/kWp per day potentially can be generated through the installed PV capacity over the long term at the optimum tilt of 11° for the PV modules.

With the high illuminance, the solar cell system is expected to generate highly efficient electric energy [23, 24] for powering the extensometer and the gateway system (including the rain gauge system). The developed solar system comprises solar panels, an MPPT (maximum-power-point-tracking) charge controller, and batteries, as illustrated in Fig 6 (a). Table I and Table II summarize the specifications of the applied solar-energy system for the gateway and the extensometer systems, respectively. A solar power characterization was firstly conducted to observe its capability before being implemented in the actual field. According to 22 days of the preliminary experiment, the solar panels' voltage profile (Fig. 6 (b)) was observed to provide a higher voltage than the battery voltage, requiring a maximum charging condition. Furthermore, under a power load of ~6 W, the performed current (Fig. 6 (c)) can completely fulfill the necessary load current during charging or discharging. Hence, the proposed power system is expected to work correctly without a power deficiency.

III. RESULT AND DISCUSSION

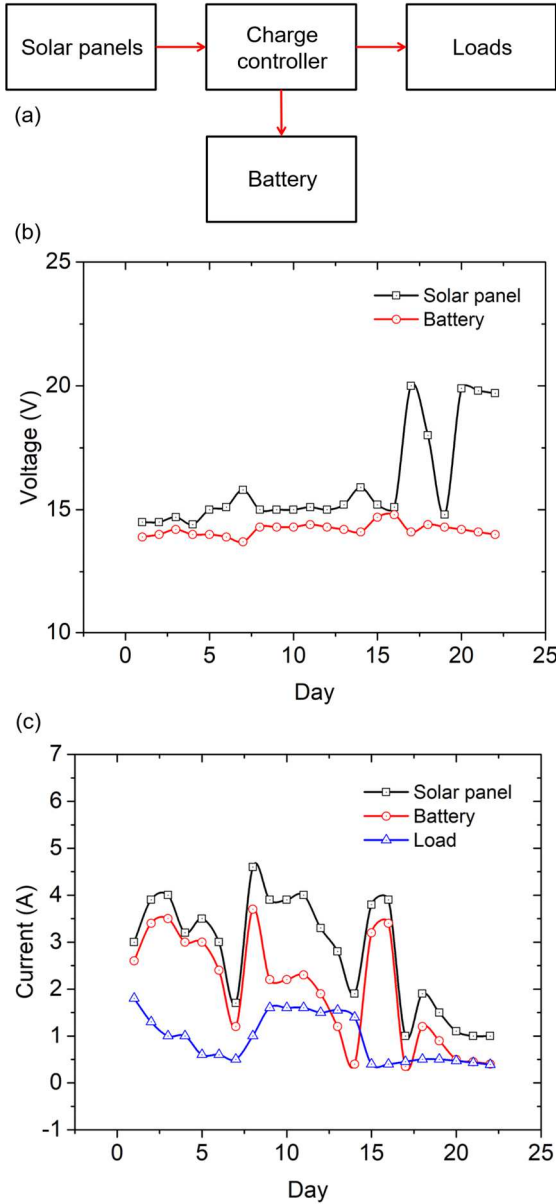


Fig. 6 (a) Schematic of a solar power system. Performance of (b) measured voltage in solar panel and battery and (c) measured current in solar panel, battery, and load side for 22 days.

TABLE I
SPECIFICATION OF GATEWAY POWER SYSTEM

Parameter	Specifications
Solar panel operating power	100 W
Solar panel operating voltage	12 V
Solar panel operating current	6 A
Battery voltage	12 V
Battery capacity	70 Ah

TABLE III
SPECIFICATION OF EXTENSOMETER POWER SYSTEM

Parameter	Specifications
Solar panel operating power	3.5 W
Solar panel operating voltage	5.5 V
Solar panel operating current	0.54 A
Battery voltage	3.7 V
Battery capacity	9.3 Ah

To examine the designed extensometer, we installed this device in a landslide-prone area that faced a railroad KM-107 area in Purwakarta reGENCY, West Java, Indonesia (-6.6, 107.4), as mapped in Fig. 7. According to the physical analysis and direct investigation, this area has an unstable soil structure. Multiyear efforts in diminishing the landmass of the pitch apparently could not entirely discontinue the land movement. The steep slope with a vast continent could not be easily transported in a short time; therefore, this effort is necessarily accompanied by continuous landslide monitoring as a supporting reference during these mitigation works. In regard, the extensometer is perceived to deserve for performing the monitoring work, especially detecting the translational land movement. The extensometer was installed by first identifying a land fracture between motion and motionless parts of the land. Fig. 8 illustrates how the extensometer is planted in the unmoving land, and subsequently, its sling rope (wire) is pulled away by a certain distance to the moving soil part. A shifting of the moving soil is expected to result in a translational motion, which is subsequently can be measured by the extensometer.



Fig. 7 Location of extensometer installation in the prone landslide area facing a double-track train road.

Before the real implementation, characterization of the employed extensometer was conducted. As shown in Fig 9, a linear relation R-squared of 0.9998 between translation shift of 5 mm with pulse numbers is achieved within 200 mm of the total shift. An equation of $y = 0.0036x + 0.11354$ is subsequently deployed to the microcontroller system for calculating the soil shift of each change of pulse counter. With the specification of 2000 pulses/rotation of each photodetector, this wire extensometer can exhibit a resolution of 0.011 ± 0.0083 mm, which is preferable to the resolution shown by a commercial wire extensometer from OTR. Ltd, i.e., 0.03 mm [25]. Moreover, a speed limit of about 36 mm/s was identified under a speed counter of 1 kHz used in the microcontroller system. The pulses will not recognize if the translation speed exceeds the speed limit and eventually lead to inaccurate shift measurement. However, in the context of debris flow, the landslide speed is typically ~ 4.5 mm/s.

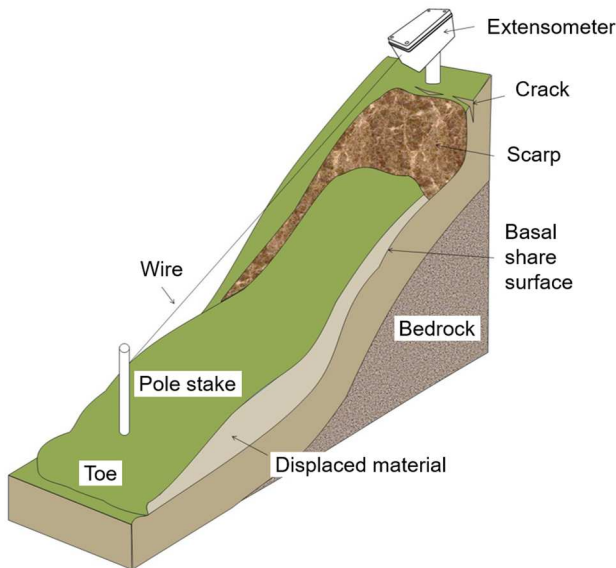


Fig. 8 Illustration of extensometer installation planted in the un-moving ground and further connected to the motion ground through a sling rope.

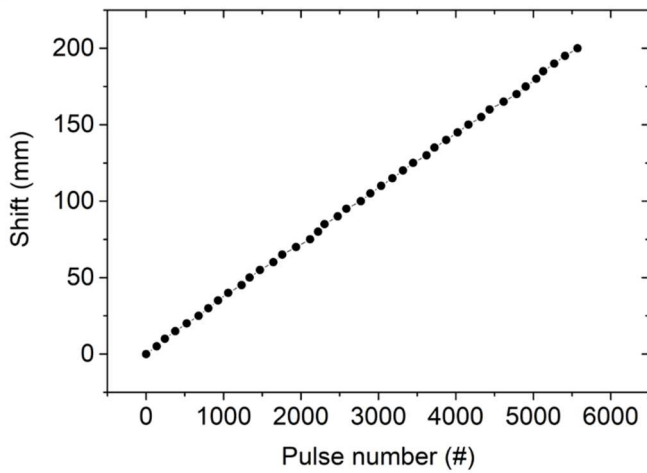


Fig. 9 Illustration of extensometer installation planted in the un-moving ground and further connected to the motion ground through a sling rope.

As the measurement results in the field, Fig. 10 demonstrates a slight soil movement/shifting of ~ 12 mm obtained from the 1st observation spot led to a sliding rate of ~ 0.25 mm/h. While on the 2nd spot, a more extensive slide was recorded at about 150 mm and demonstrated a sliding rate of ~ 4.2 mm/h. Both slides showed these two spots distinctly initiated by a pretty high rainfall of 2 - 12 mm. As described in [26–29], rainfall infiltration was considered a significant triggering factor to induce the landslide due to able to increase the pore-water pressure and causes the rising of the groundwater table [30, 31]. According to the obtained results, water infiltration was suspected of driving the landslide in the observed area.

Furthermore, an actual investigation was conducted to confirm the measurement results with the existing field condition. Firstly, we found some wellsprings appearance in the observed area, which is supposed to be due to high rainfall. Furthermore, as shown in Fig. 11, a significant soil fraction of ~ 50 mm and ~ 500 mm at the 1st and 2nd locations were discovered. The unsuitability between the measured slide with the actual observation in those two spots is supposedly due to

the stake moving sideways. A combination of translational soil movement with the rotational soil movement [32] is alleged to contribute to the unexpected stake movement, which here a pure translation is desired.

Furthermore, a pretty big step of subsidence is found in the surface around the stake that is usually found in a rotational landslide [33] and may not deliver a pure translation landslide, which is expected to pull the sling rope linearly. Moreover, some other factors, such as thickness, depth, and dip angle of the landslide surface [34, 35], can be attributed to this deviation (unsuitability). Therefore, to improve the accuracy, the analysis is suggested to involve the soil's rotational information by integrating a rotational sensor (e.g., gyroscope), and then the water content is preferred to be detected as well.

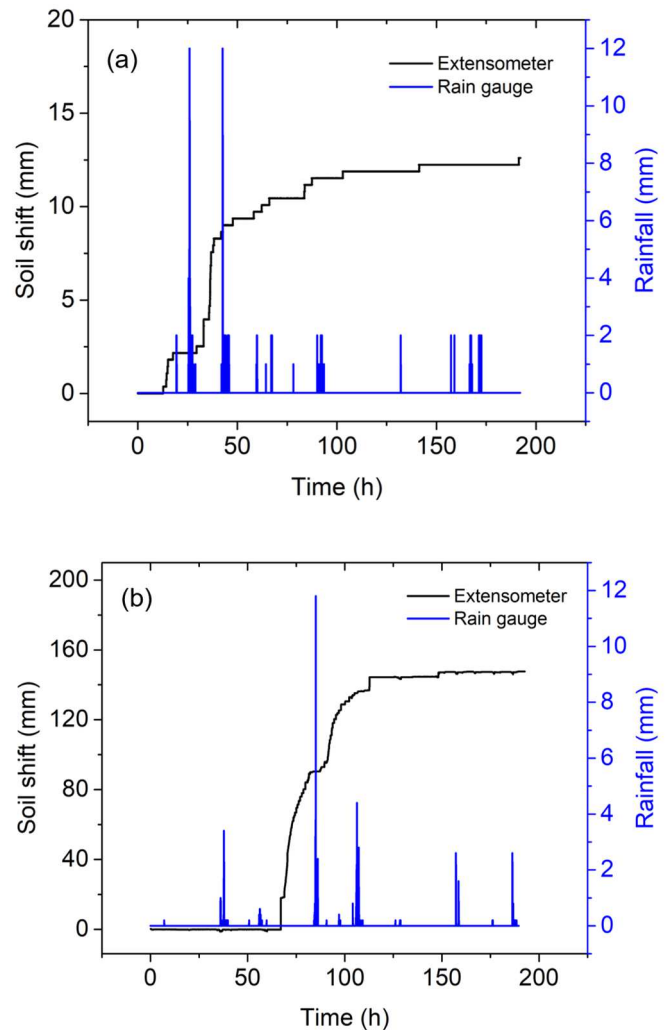


Fig. 10 Measurement results of extensometer at (a) the 1st -spot and (b) the 2nd -spot showing a soil shift of ~ 12 mm and ~ 150 mm. Both of these shifting soil mainly triggered by a quite large rainfall measured around 12 mm for both cases.

As confirmed, compared to the soil shift at the 1st spot, a more significant land fraction was found at the 2nd spot. Here, a more significant fraction's appearance at the 2nd spot is understandable since this spot is a steep slope with more heavy soil material, which is prone to be the slide. On the contrary, the 1st spot is a pretty flat area with a slow slide that tends to exhibit a type of spreads landslide. This slide type

may result from liquefaction or flow (and extrusion) of the softer underlying material [36, 37]. Overall, the extensometer can properly confirm the soil displacement occurrence in the actual spot.



Fig. 11 Actual investigation on the measurement spot showing soil shift of ~ 50 mm and ~ 500 mm at the 1st-spot and the 2nd-spot, respectively.

In addition, the recorded voltage measurements of the battery connected to the extensometer and the gateway system exhibit a charging and discharging daily cycle. The voltage performance can be appropriately maintained at 4.1 ± 0.01 V and 13.6 ± 0.53 V. Hence, the supplied power was sufficient to continuously supply the deployed remote system. As a final remark, the designed extensometer allied with the wireless network system could work properly to detect soil displacement and be considered implemented in the landslide early warning monitoring system.

IV. CONCLUSION

This work has implemented encoder-based wire extensometers in the landslide-prone area. The developed wireless network system can collect and transmit the data appropriately to the cloud system for analysis. Moreover, the wire extensometer exhibited a positive performance and

delivered some confirmed soil shifting. However, due to any variation of landslide type, the extensometer measurement is seemingly insufficient to quantify the soil shifting accurately. Other parameters, such as soil rotation and water content, are supposedly necessary to be considered. These parameters are intended to describe the actual landslide condition overall and accurately predict the soil shift.

ACKNOWLEDGMENT

This project received funding from the Ministry of Research and Technology of the Republic of Indonesia and was supported by the Research and Development Agency of Transportation of the Ministry of Transportation.

REFERENCES

- [1] J. Guo, J. Wang, Y. Li, and S. Yi, "Discussions on the transformation conditions of Wangcang landslide-induced debris flow," *Landslides*, vol. 18, no. 5, pp. 1833–1843, 2021, doi: 10.1007/s10346-021-01650-4.
- [2] M. Chang, C. Luo, B. Wu, and L. Xiang, "Catastrophe process of outburst debris flow triggered by the landslide dam failure," *Journal of Hydrology*, vol. 609, no. 3, p. 127729, 2022, doi: 10.1016/j.jhydrol.2022.127729.
- [3] S. A. Sepúlveda, S. M. Moreiras, D. Chacón, T. Villaseñor, P. Jeanneret, and F. Poblete, "The Pangal landslide complex, Cachapoal basin, central Chile (34°S): An example of a multi-temporal slope instability cluster in the Andes," *Journal of South American Earth Sciences*, vol. 115, 3–4, p. 103769, 2022, doi: 10.1016/j.jsames.2022.103769.
- [4] X. Wang *et al.*, "Relationship between the spatial distribution of landslides and rock mass strength, and implications for the driving mechanism of landslides in tectonically active mountain ranges," *Engineering Geology*, vol. 292, no. 5236, p. 106281, 2021, doi: 10.1016/j.enggeo.2021.106281.
- [5] Y. R. M and B. Dolui, "Statistical and machine intelligence based model for landslide susceptibility mapping of Nilgiri district in India," *Environmental Challenges*, vol. 5, p. 100211, 2021, doi: 10.1016/j.envc.2021.100211.
- [6] K. Šilhán, "The dendrogeomorphic spatio-temporal reconstruction of flow-like landslides activity in one of the most susceptible region of Central Europe (the Vsetínské vrchy Mts.)," *Dendrochronologia*, vol. 67, p. 125830, 2021, doi: 10.1016/j.dendro.2021.125830.
- [7] J. A. Watkins, B. L. Ehlmann, and A. Yin, "Spatiotemporal evolution, mineralogical composition, and transport mechanisms of long-runout landslides in Valles Marineris, Mars," *Icarus*, vol. 350, no. 4, p. 113836, 2020, doi: 10.1016/j.icarus.2020.113836.
- [8] David Milne Cruden, D.J. Varnes, *Landslide Types and Processes*: National Research Council, Transportation Research Board, 1996.
- [9] Y. Du, M. Xie, and J. Jia, "Stepped settlement: A possible mechanism for translational landslides," *CATENA*, vol. 187, no. 03, p. 104365, 2020, doi: 10.1016/j.catena.2019.104365.
- [10] J. Xie *et al.*, "Predicting the sliding behavior of rotational landslides based on the tilting measurement of the slope surface," *Engineering Geology*, vol. 269, no. 2, p. 105554, 2020, doi: 10.1016/j.enggeo.2020.105554.
- [11] B.-G. Chae, H.-J. Park, F. Catani, A. Simoni, and M. Berti, "Landslide prediction, monitoring and early warning: a concise review of state-of-the-art," *Geosci J*, vol. 21, no. 6, pp. 1033–1070, 2017, doi: 10.1007/s12303-017-0034-4.
- [12] Y. Xu *et al.*, "Landslide monitoring and runout hazard assessment by integrating multi-source remote sensing and numerical models: an application to the Gold Basin landslide complex, northern Washington," *Landslides*, vol. 18, no. 3, pp. 1131–1141, 2021, doi: 10.1007/s10346-020-01533-0.
- [13] R. Khan, S. Yousaf, A. Haseeb, and M. I. Uddin, "Exploring a Design of Landslide Monitoring System," *Complexity*, vol. 2021, no. 2, pp. 1–13, 2021, doi: 10.1155/2021/5552417.
- [14] B. Zhang and Y. Wang, "An Improved Two-Step Multitemporal SAR Interferometry Method for Precursory Slope Deformation Detection Over Nanyu Landslide," *IEEE Geosci. Remote Sensing Lett.*, vol. 18, no. 4, pp. 592–596, 2021, doi: 10.1109/LGRS.2020.2981146.

- [15] G. Aslan, M. Fomelis, D. Raucoules, M. de Michele, S. Bernardie, and Z. Cakir, "Landslide Mapping and Monitoring Using Persistent Scatterer Interferometry (PSI) Technique in the French Alps," *Remote Sensing*, vol. 12, no. 8, p. 1305, 2020, doi: 10.3390/rs12081305.
- [16] Y. Wang *et al.*, "On the applicability of satellite SAR interferometry to landslide hazards detection in hilly areas: a case study of Shuicheng, Guizhou in Southwest China," *Landslides*, vol. 226, p. 20, 2021, doi: 10.1007/s10346-021-01648-y.
- [17] C. Chen, M.-w. Xie, Y.-j. Jiang, B.-n. Jia, and Y. Du, "A new method for quantitative identification of potential landslide," *Soils and Foundations*, vol. 61, no. 5, pp. 1475–1479, 2021, doi: 10.1016/j.sandf.2021.07.004.
- [18] Sukristiyanti, K. Wikantika, I. A. Sadisun, L. F. Yayasanman, A. Tohari, and M. H. Zaenal Putra, "Evaluation of Parameter Selection in the Bivariate Statistical-based Landslide Susceptibility Modeling (Case Study: the Citarik Sub-watershed, Indonesia)," *International Journal on Advanced Science, Engineering and Information Technology*, vol. 12, no. 1, p. 244, 2022, doi: 10.18517/ijaseit.12.1.14737.
- [19] M. Chen and Q. Jiang, "An early warning system integrating time-of-failure analysis and alert procedure for slope failures," *Engineering Geology*, vol. 272, no. 2, p. 105629, 2020, doi: 10.1016/j.enggeo.2020.105629.
- [20] M. Chen, D. Huang, and Q. Jiang, "Slope movement classification and new insights into failure prediction based on landslide deformation evolution," *International Journal of Rock Mechanics and Mining Sciences*, vol. 141, no. 6, p. 104733, 2021, doi: 10.1016/j.ijrmm.2021.104733.
- [21] D. Bayuwati, I. Mulyanto, B. Widiyatmoko, M. I. Afandi, Suryadi, and E. Kurniawan, "Investigation on a macro bending based-fiber extensometer as displacement sensor with light source modulation for power supply efficiency," in *International Conference on Trends in Material Science and Inventive Materials: ICTMIM 2020*, Coimbatore, India, 2020, p. 20004.
- [22] M. Arsyad, R. M. Alghifari, A. Susanto, P. Palloan, and Sulistiawaty, "Analysis of Radiation Intensity and Sunshine Duration in the Karst Area of Maros TN Bantimurung Bulusaraung South Sulawesi During Solstice Phenomenon," *jppipa, pendidikan ipa, fisika, biologi, kimia*, vol. 7, SpecialIssue, pp. 199–204, 2021, doi: 10.29303/jppipa.v7iSpecialIssue.1068.
- [23] C. Yang, R. Xue, X. Li, X. Zhang, and Z. Wu, "Power performance of solar energy harvesting system under typical indoor light sources," *Renewable Energy*, vol. 161, no. 12, pp. 836–845, 2020, doi: 10.1016/j.renene.2020.06.088.
- [24] G. Lee, M. Shin, G. y. Lee, and H. Ko, "High-efficiency white-light solar window using waveguide glass plate," *Energy and Buildings*, vol. 202, p. 109341, 2019, doi: 10.1016/j.enbuild.2019.109341.
- [25] OTR-GEO, *Wire Extensometer*. [Online]. Available: http://www.otr-geo.com/PDF_ENG/Wire_Extensometer-ENG.pdf (accessed: May 6th 2021).
- [26] S. Alsubal, N. b. Sapari, I. S.H. Harahap, and M. Ali Mohammed Al-Bared, "A review on mechanism of rainwater in triggering landslide," *IOP Conf. Ser.: Mater. Sci. Eng.*, vol. 513, p. 12009, 2019, doi: 10.1088/1757-899X/513/1/012009.
- [27] M. Li *et al.*, "Warning of Rainfall-Induced Landslide in Bazhou District," in *IGARSS 2020 - 2020 IEEE International Geoscience and Remote Sensing Symposium*, Waikoloa, HI, USA, Sep. 2020 - Oct. 2020, pp. 6879–6882.
- [28] M. R. Sheikh, Y. Nakata, M. Shitano, and M. Kaneko, "Rainfall-induced unstable slope monitoring and early warning through tilt sensors," *Soils and Foundations*, vol. 61, no. 4, pp. 1033–1053, 2021, doi: 10.1016/j.sandf.2021.05.010.
- [29] F. Huang, J. Chen, W. Liu, J. Huang, H. Hong, and W. Chen, "Regional rainfall-induced landslide hazard warning based on landslide susceptibility mapping and a critical rainfall threshold," *Geomorphology*, vol. 408, no. 3, p. 108236, 2022, doi: 10.1016/j.geomorph.2022.108236.
- [30] P. van Tien *et al.*, "Rainfall-induced catastrophic landslide in Quang Tri Province: the deadliest single landslide event in Vietnam in 2020," *Landslides*, vol. 36, no. 2, p. 121, 2021, doi: 10.1007/s10346-021-01664-y.
- [31] D. Notti *et al.*, "A multidisciplinary investigation of deep-seated landslide reactivation triggered by an extreme rainfall event: a case study of the Monesi di Mendatica landslide, Ligurian Alps," *Landslides*, vol. 11, p. 1, 2021, doi: 10.1007/s10346-021-01651-3.
- [32] P. Xin, Z. Liu, S.-r. Wu, C. Liang, and C. Lin, "Rotational-translational landslides in the neogene basins at the northeast margin of the Tibetan Plateau," *Engineering Geology*, vol. 244, no. 2, pp. 107–115, 2018, doi: 10.1016/j.enggeo.2018.07.024.
- [33] I. Zapico, A. Molina, J. B. Laronne, L. Sánchez Castillo, and J. F. Martín Duque, "Stabilization by geomorphic reclamation of a rotational landslide in an abandoned mine next to the Alto Tajo Natural Park," *Engineering Geology*, vol. 264, no. 5, p. 105321, 2020, doi: 10.1016/j.enggeo.2019.105321.
- [34] J. Corominas *et al.*, "Measurement of landslide displacements using a wire extensometer," *Engineering Geology*, vol. 55, no. 3, pp. 149–166, 2000, doi: 10.1016/S0013-7952(99)00086-1.
- [35] C.-H. Tseng, Y.-C. Chan, C.-J. Jeng, R.-J. Rau, and Y.-C. Hsieh, "Deformation of landslide revealed by long-term surficial monitoring: A case study of slow movement of a dip slope in northern Taiwan," *Engineering Geology*, vol. 284, no. 2, p. 106020, 2021, doi: 10.1016/j.enggeo.2021.106020.
- [36] G. B. Crosta, S. Imposimato, and D. Roddeman, "Landslide Spreading, Impulse Water Waves and Modelling of the Vajont Rockslide," *Rock Mech Rock Eng*, vol. 49, no. 6, pp. 2413–2436, 2016, doi: 10.1007/s00603-015-0769-z.
- [37] W. Liu, W. Chen, Q. Wang, J. Wang, and G. Lin, "Effect of pre-dynamic loading on static liquefaction of undisturbed loess," *Soil Dynamics and Earthquake Engineering*, vol. 130, no. 1, p. 105915, 2020, doi: 10.1016/j.soildyn.2019.105915.